Neurosci. Bull. September, 2026, 42(9):2151–2156
https://doi.org/10.1007/s12264-026-01654-x

www.neurosci.cn
www.springer.com/12264

LETTER TO THE EDITOR

Real-Time Monitoring of Anaesthetic-Induced Change of Consciousness States Associated with Brain Biophoton Information Integration

Na Liu[1,2] · Qiao Wei[1,2] · Chengming Xia[1,2] · Jinzhong Li[1,2] · Chunli Qin[1,2] · Yan Sun[1,2] · Zhuo Wang[3] · Hao Lei[4] · Jiapei Dai[1,2]

Received: 26 November 2025 / Accepted: 24 April 2026 / Published online: 26 June 2026
© Center for Excellence in Brain Science and Intelligence Technology, Chinese Academy of Sciences 2026

Dear Editor,

Although various theories currently attempt to explain the emergence of consciousness, numerous mysteries remain unresolved. Key challenges in validating these theories include identifying the neural correlations of consciousness and addressing both the "easy" and "hard" problems it presents [1, 2]. Therefore, advancing our understanding of the origin and mechanisms of consciousness requires not only theoretical development but also breakthroughs in research technology. Recent research suggests that biophoton emissions in brain slices, also known as ultraweak photon emissions (UPE)—a form of unconventional photons found in living organisms and distinct from traditional electromagnetic activity—may play a crucial role in information transmission within the brain's neural circuits [3–5]. This implies that the brain could function as a "light information center processor," enabling complex brain functions with exceptionally low energy consumption [6, 7]. These findings provide an important source of neural information, paving the way for new technologies aimed at detecting and assessing conscious activities.

Here, we report a technology for the real-time monitoring of biophotonic emissions in the cortical areas of live rats (Fig. S1A). By employing two types of general anesthesia to establish rat models of consciousness "global state" transitions, we observed characteristic changes in biophotonic emissions in the cerebral cortex of rats, focusing on areas responsible for integrated motor and sensory functions under normal and anesthesia-associated states, corresponding to altered states of consciousness: wakefulness, unconsciousness, the transition to consciousness recovery, and fully recovered consciousness.

To build biophoton detection technology for the *in vivo* rat brain, the core component of this technology is a multimodal, high-transmittance optical fiber bundle (comprising 20 optical fibers) of an appropriate size, which can be connected to an optic-fiber bundle docking sleeve fixed on the animal's skull or a cranial window (Fig. S1B and C). This design addresses the challenge posed by the extremely weak intensity of biophotons emitted spontaneously by the brain, where a single optical fiber or a small bundle cannot sufficiently detect emissions from functional areas of the rat brain. Additionally, an excessively large optic-fiber bundle is impractical for rat skull fixation. Another key technical requirement is that the optic-fiber bundle docking sleeve fixed on the skull must ensure complete light shielding to prevent interference from ambient light, maintain a high signal-to-noise ratio (SNR) for biophoton detection, and allow for repeated measurements in model rats. Furthermore, building on our previously developed ultra-weak biophotonic imaging system (UBIS), a photomultiplier tube (PMT, a spectral detection range of 300–650 nm) was used instead of EMCCD cameras for imaging, and was housed in a dark box to enhance experimental convenience and

Supplementary Information The online version contains supplementary material available at https://doi.org/10.1007/s12264-026-01654-x.

✉ Jiapei Dai
jdai@mail.scuec.edu.cn

1 Wuhan Institute for Neuroscience and Neuroengineering, South-Central Minzu University, Wuhan 430074, China

2 The College of Life Sciences, South-Central Minzu University, Wuhan 430074, China

3 Medical Science Research Center, Zhongnan Hospital of Wuhan University, Wuhan 430071, China

4 The Innovation Academy for Precision Measurement Science and Technology, Chinese Academy of Sciences, Wuhan 430071, China

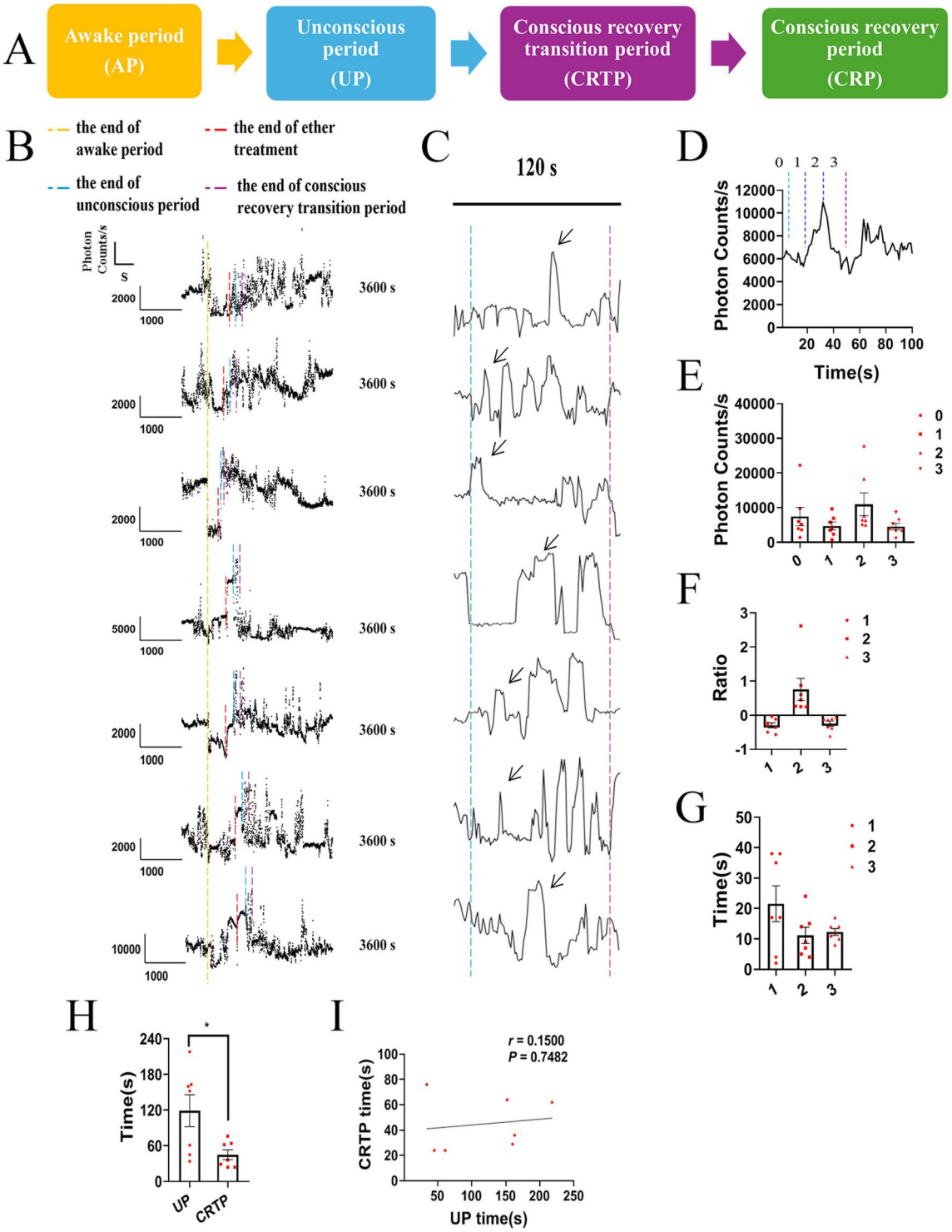

enable real-time signal display. This system provides stable background photon counts at an extremely low level of approximately 50 counts per second (50 ± 0.6, $n = 3$). When an ultra-weak white LED light beam (~3600 counts/s) was used to irradiate one end of the optic-fiber bundle, the photon count at the other end was approximately 1250 counts/s (1250 ± 3.7, $n = 3$), yielding an acquisition efficiency of about 35% (Fig. S1D), which meets the requirements for biophoton detection. We also evaluated the light shielding performance of the optic-fiber bundle docking sleeve by measuring biophotonic emissions in the cerebral cortex of the same rat, both in living and post-mortem states (within 10 min of cardiac arrest) through a cranial window. The mean biophotonic emissions detected in the cortex of

◂**Fig. 1** Dynamic changes in biophotonic emissions during ether anesthesia without craniotomy. **A** Schematic diagram illustrating anesthesia treatment and altered states of consciousness. The abbreviations are suitable for other related picture panels in this figure. **B** Dynamic changes in biophotonic emissions across different states of consciousness in seven rats (time and intensity indicated in the upper left coordinate). **C** Biophotonic emissions during the 120-s consciousness recovery transition, with arrows marking the first characteristic peak wave observed in each animal. **D** The curve of average photon counts of consciousness recovery transition ($n = 7$). Overlay of biophotonic emissions 30 s before and 69 s after the first high peak during the consciousness recovery transition. The numbers 0–3 denote periods of change in biophotonic emissions, highlighting a high-intensity peak in the middle stage (period 2). **E**, **F** Comparison of average intensity of biophotonic emissions between the initial segment (number 0) and the subsequent three segments (numbers 1–3) during the conscious recovery transition (E), along with their difference ratio (**F**) ($n = 7$). **G** Comparison of the durations of the last three segments (numbers 1–3) during the conscious recovery transition ($n = 7$). **H**, **I** The duration of the unconscious phase and the conscious recovery transition phase (**H**) ($n = 7$), Pearson correlation analysis between the duration of the unconscious phase and the conscious recovery transition phase ($r = 0.1500$, $P = 0.7428$) (**I**). AP: awake period (yellow); UP: unconsciousness period (blue); CRTP: consciousness recovery transition period (purple); CRP: consciousness recovery period (green). Data show mean ± SEM. *Indicates $P < 0.05$; **Indicates $P < 0.01$ (two-tailed paired *t*-test).

deceased rats were significantly lower (~776 counts/s) than those in the living state (~4576 counts/s) (Fig. S1E). The corresponding SNR reached 8.6, demonstrating the excellent light-shielding capability of the optic-fiber bundle docking sleeve. In addition, to eliminate the possibility that abnormal photon emission signals might be introduced by mechanical displacement at the fiber-optic-skull interface, we simulated irregular head movements—similar to those that occur during the recovery of consciousness—in rats under deep anesthesia, while simultaneously performing brain biophoton detection. The results showed no significant changes in biophoton emission during these simulated movements (Fig. S1F). Thus, this technology offers a stable, real-time platform for detecting biophotonic emissions in the rat brain *in vivo*, providing a tool for studying advanced brain functions.

To induce changes in consciousness levels, we employed two well-established experimental strategies under general anesthesia. The first involved traditional ether inhalation, which facilitates a rapid transition from wakefulness to unconsciousness and subsequent recovery (Video S1). The second involved intraperitoneal injection of a 10% chloral hydrate solution, which allows for a slower transition through these stages (Video S2). Behavioral video recordings were used to evaluate the anesthesia-associated states in rats during anesthesia, following a modified evaluation standard based on previous reports [8–10]. Additionally, we compared biophotonic emissions in the targeted brain region under conditions with and without a skull window (craniotomy vs. non-craniotomy), providing experimental evidence for the broader, more convenient application of this technology.

In the ether anesthesia experiments, during transitions from wakefulness to unconsciousness and full consciousness recovery, through consciousness recovery transition (Figs. 1A and S2A), we observed significant characteristic changes in biophotonic emissions both without (Fig. 1, Fig. S3A, B) and with (Fig. S2, S3C, D) skull fenestration: (1) During the wakefulness period, biophotonic emissions showed low-intensity fluctuations (Figs. 1B, S2B), with an average photon count of 4504.29 counts/s (4504.29 ± 943.74, $n = 7$, Fig. S3A, Table S1) and 14057.62 counts/s (14057.62 ± 2891.69, $n = 6$, Fig. S3C, Table S1). (2) biophotonic emissions decreased rapidly and transiently during the early stages of anesthesia (unconscious pre-stage) (Figs. 1B and S2B), with an average photon count of approximately 3362.86 counts/s (3362.86 ± 712.69, $n = 7$) and 11036.46 counts/s (11036.46 ± 2250.37, $n = 6$). (3) Once the animals entered the unconscious state, biophotonic emissions remained stable, with low-intensity fluctuations (Figs. 1B; S2B), averaging approximately 7437.15 counts/s (7437.15 ± 2694.74, $n = 7$, Fig. S3A) and 15712.46 counts/s (15712.46 ± 5596.87, $n = 6$, Fig. S3C). (4) During the conscious recovery transition period, significant fluctuations in biophotonic emissions were observed (Figs. 1C and D, S2C and D). In the first phase of consciousness recovery (curve 1 in Fig. 1D), there was a brief decrease in emission intensity (lasting about 21.57 ± 5.88 s, $n = 7$; and 10.83 ± 8.53 s, $n = 6$) before the animal's first movement (such as head lifting or neck stretching), with an average photon count of 4690.43 counts/s (4690.43 ± 1136.65, $n = 7$, Fig. 1E and F) and 17598.83 counts/s (17598.83 ± 6476.99, $n = 6$, Fig. S2E and F), respectively, which was roughly 30% and 11% lower than the unconscious state, respectively (7437.86 ± 2648.67, $n = 7$, Fig. 1E and F; and 18205.50 ± 6282.19, $n = 6$, Fig. S2E and F, curve 0). In the second phase (curve 2 in Fig. 1D), there was a rapid and explosive increase in emissions lasting about 11.14 s (11.14 ± 2.67, $n = 7$) and 15.33 s (15.33 ± 6.90, $n = 6$), respectively, with an average photon count of 10943.86 counts/s (10943.86 ± 3308.16, $n = 7$) and 24286.17 counts/s (24286.17 ± 6143.35, $n = 6$), respectively, approximately 76% and 53% higher than during the unconscious state. In the third phase (curve 3 in Fig. 1D), a short-term decrease in biophotonic emissions lasting about 12.29 s (12.29 ± 1.13, $n = 7$) and 24.00 s (24.00 ± 4.65, $n = 6$), respectively, was observed (Figs. 1E, F, and G, S2E, F, and G). (5) After conscious recovery, animals exhibited alternating periods of activity and rest, accompanied by moderate fluctuations in biophotonic emissions (Figs. 1B and S2B). (6) No significant correlation was found between the duration of the unconscious period and the conscious recovery transition period ($r = 0.15$, $P = 0.7428$ for non-craniotomy, Fig. 1H and I; $r = 0.6710$, P

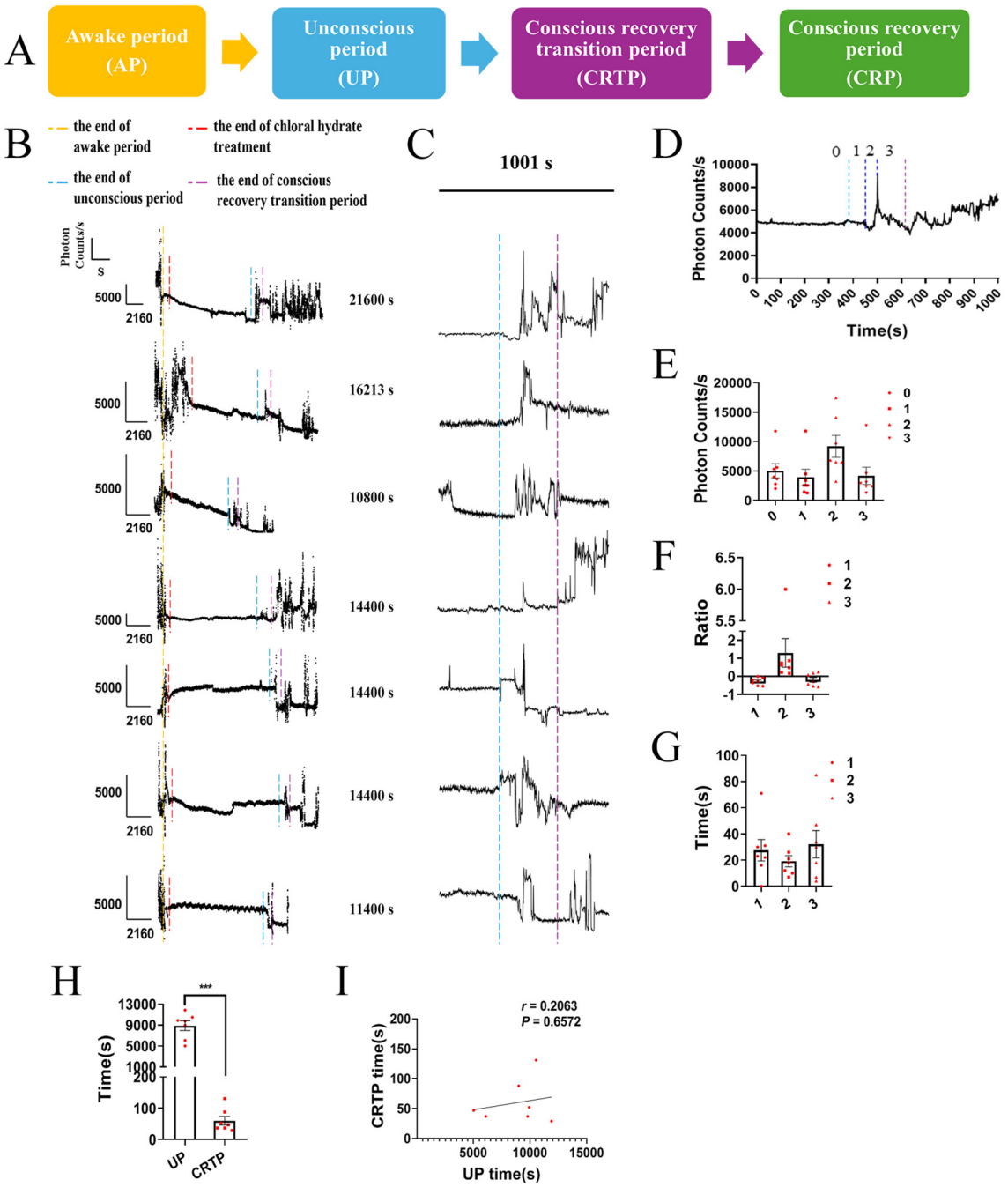

Fig. 2 Dynamic changes in biophotonic emissions during chloral hydrate anesthesia without craniotomy. **A** Schematic diagram illustrates the anesthesia treatment and the altered state of consciousness. The abbreviations are suitable for other related picture panels in this figure. **B** Dynamic changes in biophotonic emissions under different states of consciousness in seven rats (with time and intensity represented in the upper left coordinate). **C** Dynamic changes in biophotonic emissions during a 1001-s period of recovery of consciousness, with arrows indicating the first characteristic peak wave appearing in each animal. **D** The curve of average photon counts of consciousness recovery transition (n = 7). Overlay of biophotonic emissions 500 s before and 500 s after the first high peak during the consciousness recovery transition period. The numbers 0–3 indicate changes in biophotonic emissions, with a high-intensity peak observed in the mid-stage (period 2). **E**, **F** Comparison of the average intensity of biophotonic emissions between the first segment (number 0) and the other three segments (numbers 1–3) during the conscious recovery transition period (E), along with their difference ratio (**F**) (n = 7). **G** Comparison of the durations of the latter three segments (numbers 1–3) during the conscious recovery transition period (n = 7). **H**, **I** The durations of the unconscious phase and the conscious recovery transition phase (**H**) (n = 7), Pearson correlation analysis of the durations of the unconscious phase and the conscious recovery transition phase (r = 0.2063, P = 0.6572) (**I**). AP: awake period (yellow); UP: unconsciousness period (blue); CRTP: consciousness recovery transition period (purple); CRP: consciousness recovery period (green). Data show mean ± SEM. *Indicates $P < 0.05$; **indicates $P < 0.01$ (two-tailed paired t-test).

= 0.1446 for craniotomy, Fig. S2H and I). (7) Comparing the average biophotonic emission intensities across different states of consciousness, the order from high to low was unconscious period, conscious recovery transition period, conscious recovery period, and awake period (Fig. S3A and C; Table S1). However, when comparing the maximum emission values, the order from high to low was conscious recovery period, conscious recovery transition period, unconscious period, and awake period. It's also shown that the biophotonic emission maximum intensity during the consciousness recovery transition period was significantly higher than during the unconscious period (Fig. S3B and D; Table S1). (8) When comparing craniotomy versus non-craniotomy conditions, it was found that although photon counts except the unconscious period were significantly lower in the non-craniotomy group, the average and maximum biophotonic emissions across different states of consciousness showed consistency for craniotomy (Fig. S3E and F; Table S1). This indicates that the technology can effectively monitor and assess the anaesthetic-induced change of consciousness states in rats without craniotomy.

In the chloral hydrate experiments (Figs. 2, S4, and S5), we observed that the trend of changes in biophotonic emissions during the 0–3 period of consciousness recovery transition was similar to those under ether anesthesia (Figs. 2C–G and S4C–G, Table S2). The key differences are as follows: (1) After rats transitioned from wakefulness to the unconscious phase, biophotonic emissions generally showed a significant decline. However, some animals exhibited a gradual decrease (Fig. 2B, top 3 images), while others maintained a relatively stable level after the initial drop (Fig. 2B, bottom 4 images). These variations might be related to the anesthetic effects of chloral hydrate. (2) The duration of unconsciousness varied significantly among individuals (8877.29 ± 930.85 s for non-craniotomy, Fig. 2H; 6704.00 ± 1151.05 s for craniotomy, Fig. S4H, Table S2), with a slower onset and longer duration compared to ether anesthesia (Figs. 1H and S2H, Table S1). (3) The characteristic changes in biophotonic emissions during the consciousness recovery period were similar to those during the conscious state, but with smaller fluctuations than during consciousness and larger fluctuations than during unconsciousness (Figs. 2B, S4B). (4) No significant correlation was found between the duration of the unconscious period and the consciousness recovery transition period (r = 0.2063, P = 0.6572 for non-craniotomy, Fig. 2I; r = −0.6289, P = 0.1810 for craniotomy, Fig. S4I). (5) When comparing the average intensity of biophotonic emissions across different states of consciousness, it was found that the awake period exhibited higher emissions than the conscious recovery transition period, the conscious recovery period, and the unconscious period (Fig. S5A and C, Table S2). When comparing the maximum emission values, the order from high to low was the awake period, the conscious recovery period, the conscious recovery transition period, and the unconscious period (Fig. S5B and D, Table S2). (6) A comparative analysis of biophotonic emission changes under craniotomy and non-craniotomy conditions revealed similarities with ether anesthesia. In the non-craniotomy condition, aside from the overall photon count being significantly lower than that of craniotomy in the conscious recovery transition period and the conscious recovery period. The average and maximum values of biophotonic emissions in the different states of consciousness show consistency with those observed during craniotomy (Fig. S5E and F, Table S2). These distinctions from ether anesthesia suggest that chloral hydrate anesthesia continues to have residual effects after the consciousness recovery phase, preventing biophotonic emissions from returning to awake-state levels.

We employed Rényi entropy to characterize the complexity of biophotonic emissions associated with anesthesia-induced changes in consciousness states, comparing non-craniotomy and craniotomy conditions (Fig. S6). Under ether anesthesia, the magnitude of Rényi entropy H(q) decreased with increasing order q (Fig. S6A, C). During unconscious periods under non-craniotomy, the average H ($q = -1$) values were higher than those during awake, conscious recovery transition, and conscious recovery periods (Fig. S6B, Table S3). However, no significant changes in Rényi entropy were observed under craniotomy (Fig. S6D). For q = 0.5, 1, and 1.5, there were no significant differences during changes in unconscious states under either non-craniotomy or craniotomy (Fig. S6B, D). Under chloral hydrate anesthesia, H(q) also decreased as q increased (Fig. S6E, G). For $q = -1$, the unconscious state exhibited significantly lower entropy than the conscious recovery transition periods; for q = 0.5, 1, and 1.5, the entropy of the unconscious state was extremely significantly higher than that during the conscious recovery transition periods under non-craniotomy (Fig. S6F, Table S3). Some significant changes in Rényi entropy were also observed between the unconscious state and the awake periods under craniotomy (Fig. S6H, Table S3). These results demonstrate that significant differences in Rényi entropy were observed under both ether and chloral hydrate anesthesia, suggesting a potential application in monitoring anesthetic-induced changes in consciousness states.

In this study, we applied a real-time biophoton detection technology to analyze characteristic changes in brain activity during the anaesthetic-induced change of consciousness states. This provides a novel technical approach for further investigating advanced brain functions in both humans and animals, as well as offering new insights into the neural correlations of consciousness.

The analysis of human consciousness suggests that both conscious existence and altered states of consciousness are closely tied to the integration of exogenous afferent neural signals and endogenous neural information. Exogenous signals come from sensory systems such as visual, auditory,

olfactory, gustatory, somatic, and visceral inputs, while endogenous information is derived from the cortex, brainstem, and other brain regions. We demonstrated that even during the unconscious phase of animal anesthesia, a fundamental flow of biophotonic activity persists in the brain. In contrast, during the conscious phase, the consciousness recovery transition phase, and the consciousness recovery phase, different biophoton information flows appear to be integrated, potentially corresponding to the process of animal consciousness. This biophotonic activity may originate from endogenous neural circuits as well as external sensory inputs. However, further confirmation is needed, though previous studies support this hypothesis [11]. Therefore, the fundamental flow of biophotons within the brain and their transmission through neural circuits may serve as a foundation for the emergence of subconsciousness. Furthermore, our findings challenge the notion that bioelectricity is the primary medium for transmitting neural information. Specifically, the altered states of consciousness did not show a strong correlation with EEG activity [12].

Our study also revealed that the complexity of biophoton emission varies to different degrees during the process of changing consciousness states, suggesting that analyzing the radiation changes of biophotons in the brain can not only monitor and predict changes in consciousness states, but also provide new methods for studying advanced brain functions and behavioral activities in the consciousness process.

Additionally, from a speculative standpoint, the findings of this study may offer novel approaches for validating different theoretical models of consciousness and for mediating ongoing debates within the field. For instance, consciousness research has traditionally been framed by the distinction between the "easy problems"—which concern the functions and behaviors associated with consciousness—and the "hard problem"—which pertains to subjective experience and phenomenal awareness [1]. Building on this framework, four major theories of consciousness (TOCs) have emerged: higher-order theories (HOTs), global workspace theories (GWTs), integrated information theory (IIT), and theories based on re-entry and predictive processing [2]. In light of these perspectives, we speculate that intrinsic biophotonic activity in key brain regions—such as the prefrontal cortex, subcortical structures, and brainstem—may lend support to specific versions of HOTs, thereby offering new insights into the "hard problem" of consciousness. Meanwhile, the integration of biophotonic signals from various sensory modalities with intrinsic brain biophoton activity may provide novel perspectives on other theoretical models and contribute to addressing the "easy problems" of consciousness.

Overall, these findings offer a valuable approach for assessing anesthetic-induced changes in conscious states, which may have direct implications for monitoring anesthetic depth in clinical settings and for advancing the development of brain–computer interface technologies.

Acknowledgements This work was supported by the National Natural Science Foundation of China (32371155) and the Innovation Team Fund of the National Ethnic Affairs Commission (MZR20002).

Conflict of interest The authors declare no competing financial interests.

References

1. Chalmers DJ (1996) The Conscious Mind. Oxford University Press, Oxford.
2. Seth AK, Bayne T. Theories of consciousness. Nat Rev Neurosci 2022, 23: 439–452.
3. Schwabl H, Klima H. Spontaneous ultraweak photon emission from biological systems and the endogenous light field. Complement Med Res 2005, 12: 84–89.
4. Tang R, Dai J. Biophoton signal transmission and processing in the brain. J Photochem Photobiol B Biol 2014, 139: 71–75.
5. Zangari A, Micheli D, Galeazzi R, Tozzi A, Balzano V, Bellavia G. Photons detected in the active nerve by photographic technique. Sci Rep 2021, 11: 3022.
6. Wang Z, Wang N, Li Z, Xiao F, Dai J. Human high intelligence is involved in spectral redshift of biophotonic activities in the brain. Proc Natl Acad Sci U S A 2016, 113: 8753–8758.
7. Zarkeshian P, Kergan T, Ghobadi R, Nicola W, Simon C. Photons guided by axons may enable backpropagation-based learning in the brain. Sci Rep 2022, 12: 20720.
8. Mansouri MT, Fidler JA, Meng QC, Eckenhoff RG, García PS. Sex effects on behavioral markers of emergence from propofol and isoflurane anesthesia in rats. Behav Brain Res 2019, 367: 59–67.
9. Oh SS, Narver HL. Mouse and rat anesthesia and analgesia. Curr Protoc 2024, 4: e995.
10. Wang Z, Li A, Xiao G, Gu X, Wang Z, Guo S, *et al*. Unbiased segmentation and multifeature classification of cortical neuronal activity reveals complex dynamics under anesthesia. Neurosci Bull 2026, 42: 491–504.
11. Chai W, Han Z, Wang Z, Li Z, Xiao F, Sun Y, *et al*. Biophotonic activity and transmission mediated by mutual actions of neurotransmitters are involved in the origin and altered states of consciousness. Neurosci Bull 2018, 34: 534–538.
12. Mukai Y, Yamanaka A. Functional roles of REM sleep. Neurosci Res 2023, 189: 44–53.

Publisher's Note Springer Nature remains neutral with regard to jurisdictional claims in published maps and institutional affiliations.